TECHNIUM

Technium Vol. 4, Issue 6 pp.35-49 (2022)
ISSN: 2668-778X
www.techniumscience.com

Analytical Study of the Penetration of Long Rod Projectiles with Conical and Blunt Nose in Normal and Oblique Ceramic Targets

Bahman Salimi [1]*, Khodadad Vahedi [1], Amin Moslemi Petrudi [1], Masoud Rahmani [1], Ionut Cristian Scurtu [2]

[1] Department of Mechanical Engineering, Imam Hussein University, Tehran, Iran
[2] Naval Academy Mircea cel Batran Constanta
*CORRESPONDING AUTHOR: msrahmani@ihu.ac.ir

ABSTRACT: The Mechanics of penetration investigate the interactions between projectiles and targets. The Mechanics of penetration were initially developed with military motives and were used in the design and manufacture of durable military vehicles, warships, protective vests, bulletproof panels, satellite protective equipment, nuclear reactor protection used. In this paper, the penetration of cylindrical and conical-nosed long rods projectiles in normal and the diagonally ceramic target is studied by analytically and numerical methods; And the Interface defeat e phenomenon, in which the projectile is eroded so that the material in the target surface is radial and outward flow. A comparison was also made between the oblique and normal penetration of long rods cylindrical and conical-nosed projectiles, which illustrates the importance of collision angles. The analytical relations related to the reduction of velocity and erosion of the projectile mass were investigated concerning the extraction time and kinetic energy loss of the projectile. Transition from the interface defeat phase to the penetration phase is also described in detail, and the variation of the critical speed suffering from the change in the angle of impact has been investigated. Each of the results of the analytical work and numerical simulations has been evaluated by experimental work carried out in previous studies and the comparison of the results shows the acceptable accuracy for the obtained relationships.

KEYWORDS: Penetration; Long Rod Projectile; Ceramic; Conical Nose; Oblique.

1 INTRODUCTION

The issue of penetration in the military industry has a special place and so far many studies have been done in this field. Applications for penetration include the manufacture of armor, bulletproof vests, shelter design, aircraft hangars. Long rod projectiles are one of the most important projections in the discussion of heavy armor, which in this study investigates their penetration on ceramic armor and the subject of interface defeat. Researchers who studied the phenomenon of interface defeat were they studied the relationship between ballistic efficiency and compressive strength of ceramic tiles [1]. In this study, for the first time, a laboratory method for measuring the thickness of a thick ceramic backing plate was used to investigate the penetration. Their research has shown that the ballistic efficiency of ceramic targets increases with increasing effective normalized strength, a parameter defined as the average static and dynamic compressive strength of density distribution. Investigated the change in target resistance during the penetration of long rod projectiles [2]. During the collision, due to the high pressure on the contact surface of the long rod projectile with the target, the projectile material flows radially from the point of impact to the outside of the impact surface. At this time and during the interface defeat phase, there is no penetration into the ceramic. Studied the effect of metal projectiles on ceramic targets vertically [3]. They used tungsten and molybdenum projectiles and laboratorial the rate of transfer from interface defeat to penetration in a laboratory for this type of projectile. And estimated ceramic purposes of silicon carbide, boron carbide, and titanium dioxide. Investigated the dependence of the rate of penetration on the rate of impact, the results of which show a linear relationship between penetration and the rate of impact [4]. Compared interface defeat in blunt and conical projectiles vertically [5]. They calculated the formulas for reducing the velocity and erosion of the

projectile, as well as the effect of erosion of long rod projectiles in reducing kinetic energy by they have been investigated. [6]. Investigated the behavior of multilayer ceramic armor and ceramic composite armor with a formable backing plate against the anti-armor projectile "EPM 2" .The armor ceramic shows higher resistance than steel armor with the same mass [7]. Analyzed the penetration of the vertical impact of the projectile on the ceramic-metal targets in an analytical and numerical method and presented a corrective model [8]. Analyzed the impact of projectile impact on ceramic-nanocomposite hybrid targets analytically and experimentally. The results show that the use of zirconia nanoparticles in the matrix improves the ballistic performance of the particle [9]. Analyzed the effect of projectile shape on the response of orthotropic composite plates analytically and numerically, according to the results obtained in all projectiles, the maximum displacement in the center of the plate and when the layering occurs, more It has been a long time since there has been any damage. Studies and research have been conducted on the impact of projectile collisions on ceramics [10]. Conducted research in the form of reverse ballistic experiments. In these experiments, the impact of gold and tungsten projectiles on ceramic targets was investigated. They examined different ballistic functions such as penetration, interface defeat, and transition from the penetration phase to interface defeat. For velocities below this range, no penetration occurs and only interface defeat occurs; And for limited collision velocity's in this range, first interface defeat and then penetration is performed. The minimum velocity required for penetration in ceramics is called the maximum velocity, and the maximum velocity at which and lower values are only interfaced defeat is called the minimum velocity. During an interface defeat phenomenon, the projectile loses its mass; Therefore, as the mass decreases and the projectile velocity decreases, the kinetic energy and ultimately the permeability of the projectile decrease. The point to note here is that as the angle of impact increases, the upper and lower limits increase. As a result, it can be said that the pattern of mass erosion and the reduction of projectile velocity as well as the pressure on the target are different for different collision angles. According to the mentioned background in this field, studies have not been done so far in the field of the collision of projectiles with a conical nose [11]. This paper investigates the influence and phenomenon of surface failure and high-velocity, and critical times of transition from interface defeat to ceramic penetration and efficiency in oblique collisions will be discussed. Moslemi Petrudi et al. [14] Numerical and Experimental Study of Oblique Penetration of a Blunt Projectile into Ceramic- Aluminum Target. In this research, 8 experiments were carried out at the Ballistic Laboratory of Imam Hossein University and the design of the experiments was carried out in such a way that the facilities of the laboratory could be used. The results of the study showed that by increasing the angle of obliquity, is decreased substantially in ceramic-aluminum target, and when the angle of obliquity is increased beyond a certain limit, will ricochet. Also, in this study, the numerical investigation was performed, using Autodyne software. In this numerical simulation, the impact of the blunt projectile at 700 m/s on a ceramic-aluminum target was carried out to determine the penetration depth into the given target. The blunt projectile penetration was simulated with oblique carbide plates supplemented with aluminum 2024-T3 and the residual velocity and mass values of the projectile were determined at the exit of the combined target. The projectile was assumed to be rigid and the Johnson–Holmquist structural model was used to describe ceramic behavior and for projectile and target. Moslemi Petrudi et al. [15] Numerical and analytical simulation of ballistic projectile penetration due to high-velocity impact on the ceramic target.

2 ANALYSIS OF THE PENETRATION OF LONG ROD PROJECTILE WITH THE BLUNT NOSE

In Figure 1, the projectile erosion is present in the oblique collision in the form of a stable wind-blown current flowing out of the projectile surface and asymmetrically. Figure 1 shows erosion flow [11].

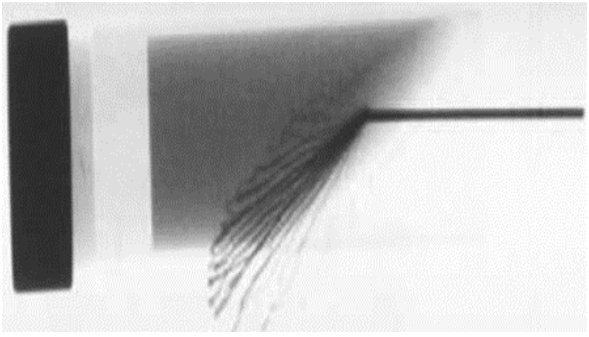

Figure 1. Erosion flow [11].

Describe the interface defeat modes for the projectile are shown with a vertical and oblique angle in figure 2.

Technium Vol. 4, Issue 6 pp.35-49 (2022)
ISSN: 2668-778X
www.techniumscience.com

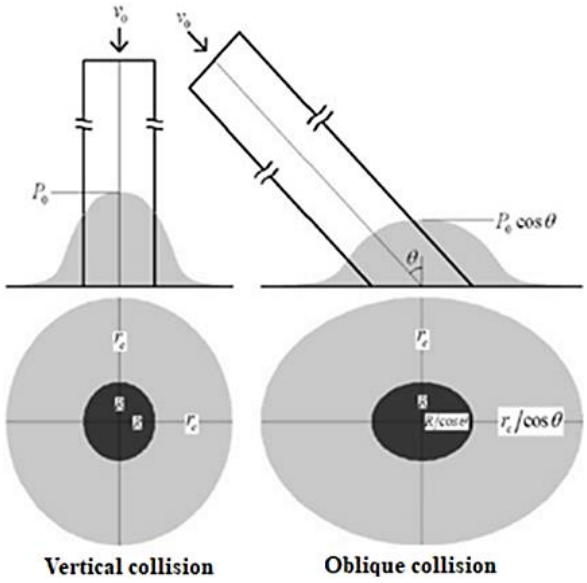

Figure 2. TheOblique and vertical collision of projectiles.

In figure 2, the collision angle θ and the projectile radius the projectile body erosion l and remain length i, so $i + l = l_0$ that l_0 is the initial length of the projectile. According to Figure 2, the interface defeat of the projectile and ceramic in the Oblique collision to elliptical, while this surface is in the form of a circle for the vertical collision. Based on Bernoulli's modified model for the penetration of long rod projectiles [12], analytical equations are presented to investigate the oblique collision of these projectiles on ceramic targets as follows:

$$(M - \rho_p \pi R^2 l) v \frac{dv}{dl} = -\sigma_{yp} \pi R^2 \quad (1)$$

$$\frac{dl}{dt} = v \quad (2)$$

In equations (1) and (2), M , the initial mass of the projectile and ρ_p , σ_{yp} , also in order of density and dynamic resistance and v , they are the velocity of the end of the projectile. According to figure (2):

$$h = l \cos\theta \quad (3)$$

So the eroded volume is equal to:

$$h = l \cos\theta \quad (4)$$

As a result, the eroded mass is equal to:

$$m = \rho_p \pi R^2 l \quad (5)$$

Therefore, according to Equation (1), the result is:

$$(M - \rho_p \pi R^2 l) v \frac{dv}{dl} = -\sigma_{yp} \pi R \frac{R}{\cos\theta} \quad (6)$$

By integrating the above relation:

$$\frac{1}{2} \rho_p (v^2 - v_0^2) = \frac{1}{\cos\theta} \sigma_{yp} \ln\left(1 - \frac{\rho_p \pi R^2 l}{M}\right) \quad (7)$$

Therefore, the relation between the projectile body erosion l and projectile velocity v can be expressed as follows:

$$l = \frac{M}{\rho_p \pi R^2} \left\{ 1 - \exp\left[\frac{\rho_p}{2\sigma_{yp}} \left(v^2 - v_0^2\right) \cos\theta \right] \right\} \quad (8)$$

By placing equation (8) in equation (6) and according to relation (2), the result is:

$$dt = -\frac{M}{\pi R \sigma_{yp}} \cos \exp\left[\frac{\rho_p}{2\sigma_{yp}}\left(v^2 - v_0^2\right)\cos\theta\right] dv \tag{9}$$

As mentioned in reference [6], the following rewards can be defined.

$$K = \frac{M v_0}{\pi R^2 \sigma_{yp}}$$
$$A = \frac{\rho_p v_0^2}{2\sigma_{yp}} \tag{10}$$

By integrating the sides of the equation (9), the relation of projectile velocity in terms of time is presented as follows.

$t = K \cos\theta . \exp(-A\cos\theta)$.

$$\int_{v/v_0}^{1} \exp\left[A\cos\theta\left(\frac{v}{v_0}\right)^2\right] d\frac{v}{v_0} \tag{11}$$

This relationship is defined for the vertical collision motion as follows [5].

$$t = K \exp(-A)\int_{v/v_0}^{1} \exp\left[A\left(\frac{v}{v}\right)^2\right] d\frac{v}{v_0} \tag{12}$$

Comparing relations (11) and (12), it is concluded that these two equations are similar; But what is important is that the variable θ enters the equation (9), which means that the angle of impact is important in reducing the projectile velocity. Equation (9) lacks an analytical solution and this equation must be solved by numerical methods. However, by solving this equation numerically, the projectile velocity can be calculated based on time. Using relation (8), the projectile body erosion of the projectile can be obtained, and then the calculated erosive mass of the projectile can be calculated. To solve equation (12) analytically, some simplifications and assumes are needed. As mentioned above, the motion of a long rod projectile during the interface defeat phase is a quasi-stable motion, and the changes in projectile velocity (v) and its reduction are negligible; Therefore, the process of reducing the projectile velocity can be approximated by a linear relation with time. Assuming $v = v_0$ the phrase can be $d\frac{v}{v_0}$ considered constant and then solved equation (11) analytically.

$$t = K\cos\theta\left(1 - \frac{v}{v_0}\right) \tag{13}$$

Therefore, the projectile velocity is expressed as follows in terms of time.

$$v = v_0 - \frac{\pi R^2 \sigma_{yp}}{M}\frac{1}{\cos\theta}t = v_0 - \frac{1}{\cos\theta}\frac{\sigma_{yp}}{\rho_p l_0}t \tag{14}$$

According to Equation (14), it can be seen that the phrase $\frac{1}{\cos\theta}$ it is related to the oblique impact motion, and it can be concluded that at equal collision velocities, the reduce the projectile velocity than the vertical motion. Using Equation (2), we can obtain the projectile body erosion in terms of time as follows:

$$l = \int_0^t v dt = v_0 t - \frac{1}{2}\frac{1}{\cos\theta}\frac{\sigma_{yp}}{\rho_p l_0}t^2 \tag{15}$$

A phrase $\frac{1}{\cos\theta}$ in Equation (15), the result is the oblique projectile motion, and its effect on Equation (15) indicates that the reduction in the projectile body in the oblique motion is slower than in the vertical motion, so the erosion rate of the projectile in the oblique motion is less than in the vertical motion. According to Equation (15), the relation of the residual mass of the projectile can be proposed in terms of such time.

Technium Vol. 4, Issue 6 pp.35-49 (2022)
ISSN: 2668-778X
www.techniumscience.com

$$m = \rho_p \pi R^2 l = M - \rho_p \pi R^2 v_0 t + \frac{1}{2}\frac{1}{\cos\theta}\frac{\pi R^2 \sigma_{yp}}{l_0} t^2 \quad (16)$$

Equation (16) indicates that the erosion rate of the projectile is lower in the oblique motion than in the vertical motion. In other words, for a projectile with the same collision velocities at a given time, the mass remaining in the collision motion is greater than in the normal collision motion.

3 ANALYSIS OF THE PENETRATION OF LONG ROD PROJECTILE WITH CONICAL NOSE

The process of eroding the mass of projectiles with a conical nose during the process of the interface defeat can be analyzed in two parts.

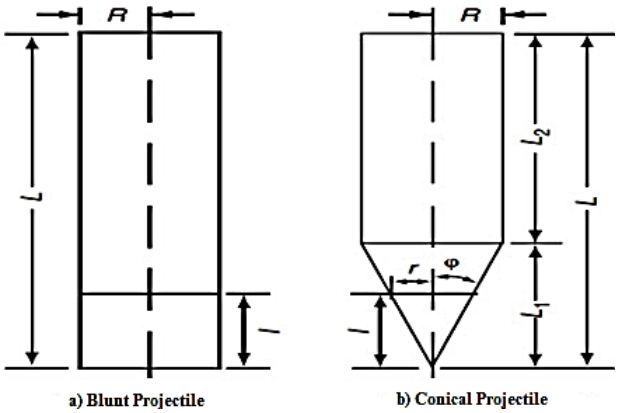

Figure 3. Schematic of two types of projectiles.

3.1 Projectile body erosion

When the head of the projectile is completely eroded, that is $l = l_1 = \frac{R}{\tan\theta}$, projectile velocity to v_1 decreases; and then the second stage of the projectile body erosion begins. The projectile body erosion is similar to the analysis of a cylindrical projectile with a blunt nose; Which was stated in the previous section; However, to analyze the process of erosion of the projectile mass in the second stage, the value $M_1 = M - \rho_g(\frac{\mu R^2 L_2}{3})$ should be used instead of the initial mass in the equations of the previous section. Initial collision velocity v_1 is considered.

3.2 Erosion nose of the projectile $l \le \frac{R}{\tan\phi}$

In the erosion stage of the projectile nose, the equation (6) can be rewritten as follows:

$$(M - \rho_p \pi R^2 l) v \frac{dv}{dl} = -\sigma_{yp}\pi\left(l\tan\varphi \times l\frac{\tan\varphi}{\cos\theta}\right) \quad (17)$$

It results in integration from the above relationship.

$$\frac{1}{2}\rho_p(v^2 - v_0^2) = \frac{1}{\cos\theta}\sigma_{yp}\ln\left(1 - \frac{\rho_p\left(\frac{1}{3}\pi l^3\tan^2\varphi\right)}{M}\right) \quad (18)$$

Thus the relation between the projectile body erosion l and projectile velocity v the following can be stated:

$$l = \left\{\frac{M}{\rho_p\left(\frac{1}{3}\pi\tan^2\varphi\right)}\left\{1 - \exp\left[\frac{\rho_p}{2\sigma_{yp}}\left(v^2 - v_0^2\right)\cos\theta\right]\right\}\right\} \quad (19)$$

By placing equation (19) in equation (18) and according to relation (2):

$$dt=\left(\frac{M{\rho_p}^2}{9{\gamma_p}^3\pi\tan^2\varphi}\right)^{\frac{1}{3}}\cos\theta\times\left\{\frac{\exp\left[\frac{\rho_p}{2\sigma_{yp}}\left(v^2-v_0^2\right)\cos\theta\right]}{\left\{1-\exp\left[\frac{\rho_p}{2\sigma_{yp}}\left(v^2-v_0^2\right)\right]\right\}^{\frac{2}{3}}}\right\}dv \tag{20}$$

As mentioned in the reference [6], the following constants can be defined.

$$K'=\left(\frac{M{\rho_p}^2}{9{\gamma_p}^3\pi\tan^2\varphi}\right)^{\frac{1}{3}}v_0$$
$$A=\frac{\rho_p v_0^2}{2\sigma_{yp}} \tag{21}$$

By integrating the sides of the equation (20), provide a relation for the velocity of the projectile in terms of time as follows.

$$t=K'\cos\theta.\exp(-\frac{1}{3}A\cos\theta).$$
$$\int_{v/v_0}^{1}\frac{\exp\left[A\cos\theta\left(\frac{v}{v_0}\right)\right]}{\exp(A\cos\theta)-\exp\left[A\left(\frac{v}{v_0}\right)^2\right]^{3/2}}d\frac{v}{v_0} \tag{22}$$

Numerical methods must be used to solve the equation (22).
By setting the value L_1 Instead l in Equation (19) the value v is calculated. This amount of calculated velocity is equal to the initial velocity in the second phase of the analysis, that is, the analysis of the projectile body.

$$\begin{cases}M_1=M-\rho_p\left(\pi R^2 L_1/3\right)\\ v=v_1\end{cases} \tag{23}$$

4 NUMERICAL SIMULATION

In this section, the numerical simulation article is used to investigate the problem of determining the critical velocity and determining the displacement of the backup layer. The boundary conditions, material model, and mesh type of each of the simulation components are shown in Table 1. Figure 4 shows **the** simulation of ricocheting the projectile. Table 2 shows **the** proportional steel material model. Table 3 shows **the** specifications of the 6061 aluminum material used in **the** simulation. Table 4 shows **the** specifications of the Al2O3 ceramic material model used in simulation [11]. Table 5 shows **the** comparison of numerical and test values [13].

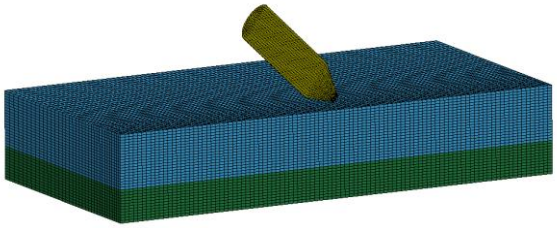

Figure 4. Simulation of ricocheting the projectile.

Table 1. Boundary conditions and simulation models.

Material	Element type	Material model	Equation of state	Boundary condition
Ceramic	Cubic	Johnson Holmquist	-	Clamp
Steel	Cubic	Johnson Cook	Mie-Gruneisen	Free
Aluminum	Cubic	Johnson Cook	Mie-Gruneisen	Clamp

The specifications for materials used in the simulation are presented in Tables 2 through 4.

Table 2. Proportional steel material model [11].

Parameter	Amount	Symbol (unit)
Density	7800	Ro ($\frac{kg}{m^3}$)
Shear modulus	80	G (GPa)
Modulus of elasticity	210	E (GPa)
Poisson's ratio	0.31	PR
Initial yield strength	507	A (Mpa)
Hardness constant	320	B (Mpa)
Strain rate constant	0.28	C
First failure parameter	0.15	D_1
Second failure parameter	0.72	D_2
Third failure parameter	1.66	D_3
Fourth failure parameter	0.005	D_4
Fifth failure parameter	-0.84	D_5
Gruneisen parameter	1.70	Γ

Table 3. Specifications of the 6061 aluminum material used in simulation [11].

Parameter	Amount	Symbol (unit)
Density	2700	Ro ($\frac{kg}{m^3}$)
Shear modulus	26	G (GPa)
Modulus of elasticity	68	E (GPa)
Poisson's ratio	0.33	PR
Initial yield strength	324	A (Mpa)
Hardness constant	114	B (Mpa)
Strain rate constant	0.002	C
First failure parameter	-0.77	D_1
Second failure parameter	1.45	D_2
Third failure parameter	-0.47	D_3
Fourth failure parameter	0	D_4
Fifth failure parameter	1.6	D_5
Gruneisen parameter	2.14	Γ

Table 4. Specifications of the Al2O3 ceramic material model used in simulation [11].

Parameter	Amount	Symbol (unit)
Density	3800	Ro ($\frac{kg}{m^3}$)
Shear modulus	0.989	G (Gpa)
Normal initial resistance	0.989	A (Gpa)
Normal failure resistance	0.77	B (Gpa)
Constant strain rate	0	C
Reference strain rate	1	EPSI(s^{-1})
Maximum tensile strength	0.15	T (Gpa)

Maximum Normal failure resistance	0.5	SFMAX
Hugoniot Elastic Limit	5.9	HEL(Gpa)
Pressure component In Hugoniot Elastic Limit	2.2	PHEL(Gpa)
Bulk modulus	200	(Gpa)K_1
Second pressure factor	0	(Gpa)K_2
Third pressure factor	0	(Gpa)K_3
Failure criterion	1.5	FS

Table 5. Comparison of numerical and test values [13].

Test number	Collision velocity (m/s)	Numerical results (mm)	Experimental results (mm)	Percentage error
1	775	14.67	14.91	1.61
2	844	16.35	17.77	7.99
3	378	8.58	7.62	12.60
4	266	6.41	7.33	12.55
5	287	6.57	6.11	7.53

Figure 5 shows the displacement of the backing layer (δ). Figure 6 shows the numerical simulation of the projectile penetration steps in the target.

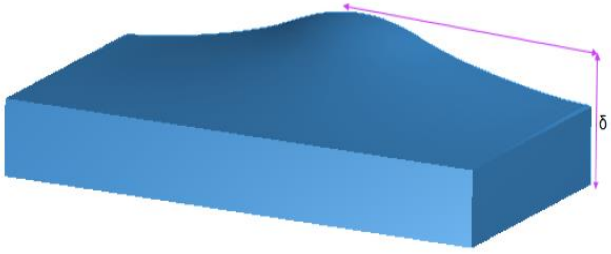

Figure 5. displacement of the backing layer (δ).

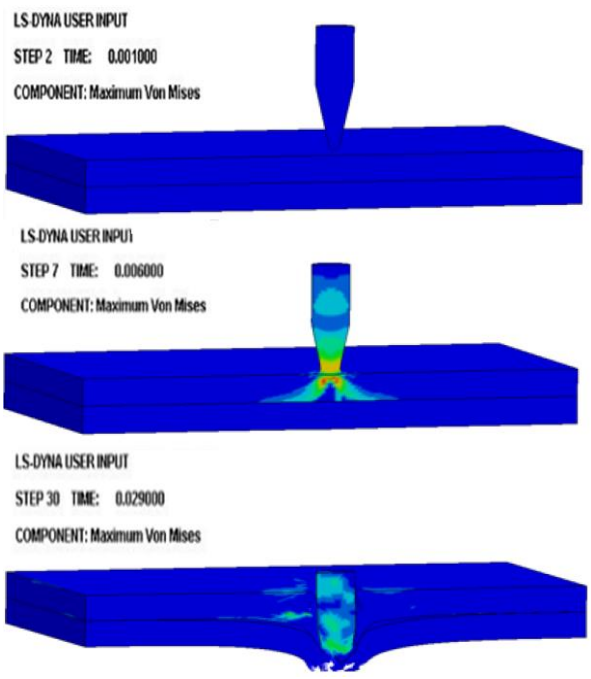

Figure 6. The vertical penetration of the projectile into the target.

5 RESULTS AND DISCUSSION

To validate the stated relations for the oblique impact of laboratory tests performed by Anderson et al. [11]. In these experiments, the impact of a long rod projectile from the properties of gold on SiC-N ceramic was performed using **the** reverse ballistic method. The projectile has a length of 70 mm and diameter of 1 mm and mechanical properties are according to Table (1).

Table 6. Characteristic of long rod projectile [9].

ρ $(\frac{kg}{m^3})$	$\sigma_{YP}(GPa)$	R(mm)	$l_0(mm)$
19300	0.09	0.5	70

The ceramic target is designed as a cylinder with a diameter of 20 mm. This cylinder is such that the angle between the upper surface and its base is 0º, 45º**,** and 60º, respectively, and the center height of this cylinder is 35 mm. The remaining length during the collision process is calculated by advanced laboratory equipment. The results of these experiments are presented in Table 7. Using Equation (19) and the parameters expressed in Table 7, the eroded length can be determined in terms of time; Also, the remaining length can be used using the relation $i = l_0 - l$, calculated for φ = 27º. Figures 4 to 6 show the results of the comparison of laboratory values [11] and the relations of analysis obtained.

Table 7. Results from Anderson experiment [10].

Collision angle	Collision velocity (m/s)	$l_0(mm)$	$t(\mu s) \mid l'(mm)$
0	766	70	15.14 | 57.69
45	928	70	6.38 | 63.57
45	1070	70	11.79 | 56.16
60	921	70	2.66 | 67.33
60	1162	70	14.12 | 54.26
60	1404	70	14.92 | 52.54

Figure 7 shows **the** comparison of residual length results in normal penetration of analytical relations calculated by experimental test for blunt projectile and conical nose projectile. Figure 8 and 9 shows **the** comparison of residual length results in 45º, 60º penetration of analytical relations calculated by experimental test for blunt projectile and conical nose projectile.

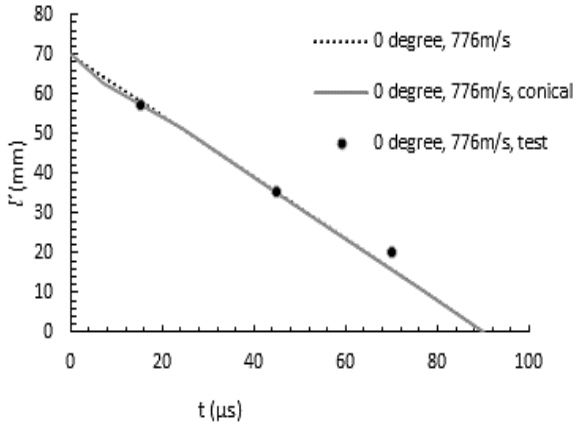

Figure 7. Comparison of residual length results in normal penetration in 0º angle.

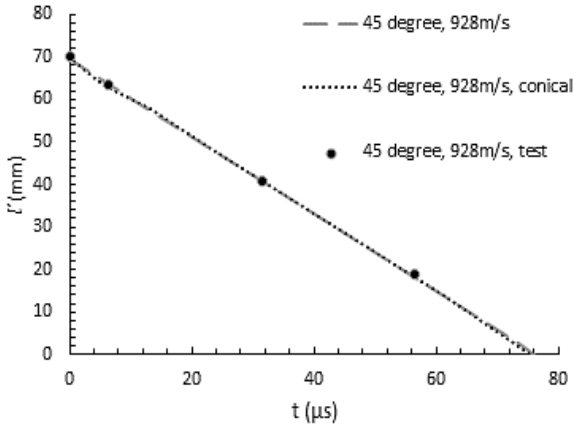

Figure 8. Comparison of residual length results in normal penetration at 45º angle.

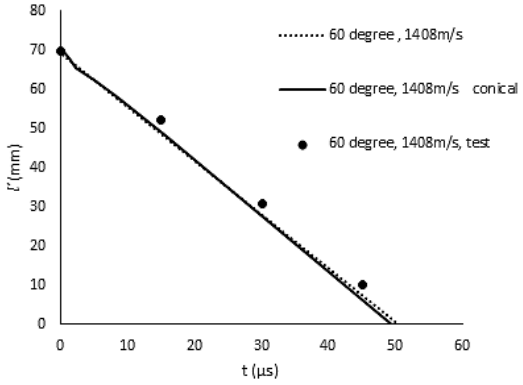

Figure 9. Comparison of residual length results in normal penetration at 60º angle.

As mentioned, in the event of a collision, the projectile decrease and the projectile erodes less than the vertical, Therefore, it can be derived that kinetic energy is equal for both vertical and oblique states. Then, using the stated analytical relations, the velocity and mass of the projectile are calculated for four different modes of velocity and collision angle, and from there, the kinetic energy for these four modes is calculated. Figures 10 and 11 show the kinetic energy of these four states. As shown in the diagram, at equal velocities, kinetic energy is equal to different angles of the collision, indicating that the reduction of kinetic energy at equal velocities is the same for different angles.

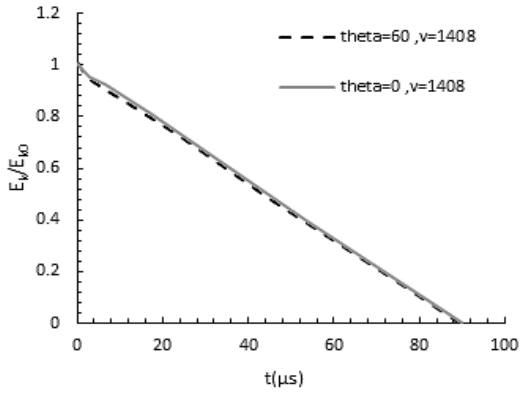

Figure 10. Diagram of kinetic energy changes for vertical collision in 60º angle at collision velocity 1408 m/s.

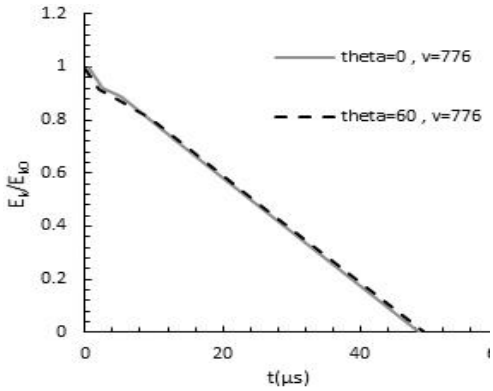

Figure 11. Diagram of kinetic energy changes for vertical collision in 60º angle at collision velocity 776 m/s.

As mentioned, the reduced kinetic energy of the projectile at different angles of impact is almost equal. One of the important effects of the collision angle is the effect of force distribution and pressure on the impact area on the projectile. Based on the results of tests performed by Anderson et al. [11], the range of critical velocit**ie**s, high limit velocity**,** and low limit velocity, increases with increasing collision angle, which is one of the important differences between oblique and vertical collisions. The pressure applied to the axis of symmetry of the projectile during vertical impact is expressed by the following equation [6].

$$p_0 = q_p\left(1+33.27\beta\right)$$
$$\beta = \frac{\sigma_{yp}}{q_p} \qquad (24)$$
$$q_p = \frac{1}{2}\rho_p v_0^{\,2}$$

In relation (24) q_p indicates projectile inertia. The geometric region of the pressure on the target plate can be shown by the following equation.

$$p_r = p_0 \cdot \sqrt{1-\left(\frac{r}{r_c}\right)^2} \qquad (25)$$

The above relation r indicates the distance from the projectile axis and r_c, the distance is critical. r_c, depends on the properties of the projectile and the target. The pressure distribution area for vertical collision **is** shown in Figure 5. Geometric pressure zone of a circle with radius r_c. Pressure on the interface of the projectile and the circular target to the radius R, much more than the pressure in the area outside the circle r_c. The pressure at which the projectile changes from vertical penetration to failure can be calculated by the following equation.

$$\sigma_{Hel} \le p_0 \le 2.85\sigma_{y0} \qquad (26)$$

The above relation σ_{Hel} indicates the elastic limit of Hugoniot's in ceramics and σ_{y0}, the initial dynamic resistance is ceramic. The relation between the two can be described as follows [14, 15, 16].

$$\sigma_{Hel} = \frac{1-\upsilon}{\left(1-2\upsilon\right)^2}\sigma_{y0} \qquad (27)$$

Concerning 27, the ratio is Poisson. By considering the relationships (24) to (27), the critical velocity range can be extracted.

$$v_0^{\,lower} = \sqrt{\frac{2\sigma_{Hel}-6.54\sigma_{yp}}{\rho_p}} \qquad (28)$$

$$v_0^{\,upper} = \sqrt{\frac{5.7\sigma y_{yo}-6.54\sigma_{yp}}{\rho_p}} \qquad (29)$$

Under oblique impact conditions, the impact surface is an oval with a large diameter $\frac{R}{\cos\theta}$ and small diameter R; As well as the pressure area as an oval with $\frac{r_c}{\cos\theta}$, r_c diameters. Therefore, energy is distributed over a wider area than perpendicular. Considering the same energy of collision in both oblique and vertical modes, concluded that the collision force is equal in both modes, so:

$$p_0'\pi r_c\left(r_c/\cos\theta\right) = p_0 r_c^{\,2} \qquad (30)$$

So the pressure from the collision is P_0' equal to:

$$p_0' = p_0 \cos\theta \tag{31}$$

Oblique impact pressure P_0', less than vertical pressure. According to equations (26) and (28), the upper and lower limit velocity's can be calculated as follows.

$$v_0^{lower'} = \frac{v_0^{lower}}{\sqrt{\cos\theta}} \tag{32}$$

$$v_0^{upper'} = \frac{v_0^{upper}}{\sqrt{\cos\theta}} \tag{33}$$

Increasing the impact angle increases the critical velocity range. Figure 12 shows the diagram of the experimental tests performed [12], the results obtained from the numerical simulation, and the results of the analysis of the obtained analyzes for different angles and the critical velocity limits. As the angle of impact increases, the critical velocity increases.

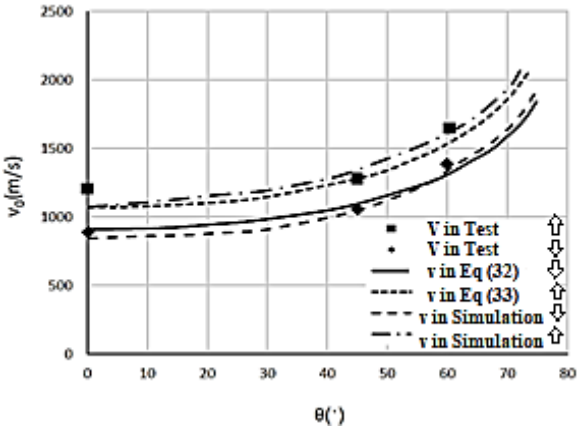

Figure 12. Comparison of critical velocity changes with the angle of collision.

According to Figure 12, there is a very good match between analytical results, numerical simulation, and experimental data, which indicates the reliability of the relations presented in this study.

6 Conclusion

According to the study and analysis in this article, it is observed that the reduction velocity of long rod projectile in collision with ceramic targets in the oblique motion is more than the vertical motion and the erosion of the mass is less than the vertical collision motion. Therefore, it is concluded that the reduction of kinetic energy in the two motions of vertical and oblique collision is not much different. Also, using the extracted relations, for projectiles with a conical nose, there is not much difference in the type of penetration and other studied parameters such as velocity reduction or mass erosion, in two types of blunt and conical projectiles. Due to the shape of the long rod projectile's head, in collision with ceramic targets at ignored high velocities. As the angle of impact increases, the critical velocity range increases, and the efficiency of projectile penetration in ceramic targets decreases. Finally, based on the relations of analysis and simulations performed, the use of ceramics that have an oblique base relative to the trajectory of the projectile increases the efficiency of the ceramic armor.

REFERENCES

[1] Rozenberg, Z., and Y. Yeshurun. "*The relation between ballistic efficiency and compressive strength of ceramic tiles*." International journal of impact engineering 7, no. 3 (1988): 357-362.
https://doi.org/10.1016/0734-743X(88)90035-8
[2] Anderson Jr, Charles E., James D. Walker, and George E. Hauver. "*Target resistance for long-rod penetration into semi-infinite targets*." Nuclear engineering and design 138, no. 1 (1992): 93-104.
https://doi.org/10.1016/0029-5493(92)90281-Y
[3] Lundberg, Patrik, René Renström, and Bengt Lundberg. "*Impact of metallic projectiles on ceramic targets: the transition between interface defeat and penetration*." International Journal of Impact Engineering 24, no. 3 (2000): 259-275.
https://doi.org/10.1016/S0734-743X(99)00152-9
[4] Orphal, D. L., and C. E. Anderson Jr. "*The dependence of penetration velocity on impact velocity*." International journal of impact engineering 33, no. 1-12 (2006): 546-554.
https://doi.org/10.1016/j.ijimpeng.2006.09.054
[5] Li, J. C., X. W. Chen, and F. Ning. "*Comparative analysis on the interface defeat between the cylindrical and conical-nosed long rods*." International Journal of Protective Structures 5, no. 1 (2014): 21-46.
https://doi.org/10.1260/2041-4196.5.1.21
[6] Li, J. C., X. W. Chen, F. Ning, and X. L. Li. "*On the transition from interface defeat to penetration in the impact of the long rod onto ceramic targets*." International Journal of Impact Engineering 83 (2015): 37-46.
https://doi.org/10.1016/j.ijimpeng.2015.04.003
[7] Yazdani, Mojtaba, and Ali Rashed. "*Studying the behavior of ceramic armors impacted by a 7.62-mm APM2 projectile*." Modares Mechanical Engineering 14, no. 14 (2015): 125-136.
https://mme.modares.ac.ir/article-15-6062-en.html
[8] Tahmaseiabdar, M, Gholam H, Hadi Sh, A. Khodadadi. "*Analytical and numerical investigation of projectile perforation into ceramic-metal targets and presenting a modified theory*." Modares Mechanical Engineering 15, no. 9 (2015): 353-359.
https://mme.modares.ac.ir/article-15-1914-en.html
[9] Shanazari, Hadi, Gholam Hossein Lighat, and Saeed Feli. "*Analysis of penetration process in hybrid ceramic/nanocomposite targets*." Modares Mechanical Engineering 16, no. 10 (2016): 137-146.
https://mme.modares.ac.ir/article-15-6319-en.html
[10] Seifoori, Sajjad, and Marzieh Hosseini. "*Analytical and Numerical study of composite plates under impact loading at low velocity with different strikers*." (2018): 53-60.
https://mme.modares.ac.ir/article-15-5970-en.html
[11] Hauver, George E., Edward J. "*Interface defeat of long-rod projectiles by ceramic armor*". ARMY RESEARCH LAB ABERDEEN PROVING GROUND MD WEAPONS AND MATERIALS RESEARCH DIRECTORATE, 2005.
https://archive.org/stream/DTIC_ADA609092/DTIC_ADA609092_djvu.txt
[12] Anderson Jr, Charles E., Thilo Behner. "*Interface defeat of long rods impacting oblique silicon carbide*". Southwest Research Inst San Antonio TX, 2011.
https://doi.org/10.1007/978-981-13-3253-1_6
[13] Moshtaghian, M., and Vahedi, K. "*Investigation and Analysis of Projectile Penetration in a Ceramic/ Composite Target*", Master's thesis of IHU University, Faculty of Engineering, 2008 (In Persian).
[14] Alekseevskii, V. P. "Penetration of a rod into a target at high velocity." Combustion, explosion, and shock waves 2, no. 2 (1966): 63-66. https://doi.org/10.1007/BF00749237
[15] Moslemi Petrudi, A., Kh Vahedi, M. H. Kamyab, and Moslemi Petrudi. "*Numerical and experimental study of oblique penetration of a blunt projectile into the ceramic-aluminum target*." Modares Mechanical Engineering 19, no. 5 (2019): 1253-1263.
https://mme.modares.ac.ir/article-15-20854-en.html
[16] Petrudi, A Moslemi, Kh Vahedi, M Rahmani, and MAliMoslemi Petrudi. "*Numerical and analytical simulation of ballistic projectile penetration due to high-velocity impact on the ceramic target*." Frattura ed Integrità Strutturale 14, no. 54 (2020): 226-248. https://doi.org/10.3221/IGF-ESIS.54.17